Filtered Dark Matter at a First Order Phase Transition

Michael J. Baker,[1,2,*] Joachim Kopp,[3,4,†] and Andrew J. Long[5,‡]

[1] *School of Physics, The University of Melbourne, Victoria 3010, Australia*
[2] *Physik-Institut, Universität Zürich, 8057 Zürich, Switzerland*
[3] *Theoretical Physics Department, CERN, Geneva, Switzerland*
[4] *PRISMA Cluster of Excellence & Mainz Institute for Theoretical Physics, Johannes Gutenberg University, Staudingerweg 7, 55099 Mainz, Germany*
[5] *Rice University, Houston, Texas 77005, USA*

(Dated: December 9, 2019)

We describe a new mechanism of dark matter production in the early Universe, based on the dynamics of a first order phase transition. We assume that dark matter particles acquire mass during the phase transition, making it energetically unfavourable for them to enter the expanding bubbles of the massive phase. Instead, most of them are reflected off the advancing bubble walls and quickly annihilate away in the massless phase. The bubbles eventually merge as the phase transition is completed, and only the dark matter particles which have entered the bubbles survive to constitute the observed dark matter today. This mechanism can produce dark matter with masses from the GeV scale to above the PeV scale, including a large region of viable parameter space beyond the Griest–Kamionkowski bound. Current and future direct detection and collider experiments can probe much of the viable parameter space.

1. Introduction. A wealth of observational evidence reveals that the universe is permeated with a mysterious substance known as dark matter (DM) [1]. Very little, however, is known about the particle physics nature of DM or its origin in the early Universe. Historically, the favoured scenario for DM production has been thermal relic production [2–4]. If a DM particle is thermalised with the Standard Model (SM) plasma in the early Universe then the cosmological expansion, which causes the plasma to cool adiabatically, will eventually make the DM's interactions with the SM inefficient, driving it out of equilibrium. Consequently, the DM relic abundance is determined when these interactions "freeze-out," typically increasing with larger DM mass and decreasing with larger interaction strength. Above $m_{\rm DM} \sim 100\,\text{TeV}$ the required interactions violate unitarity [5, 6]. This places an upper bound on the mass of thermally-produced DM, known as the Griest–Kamionkowski (GK) bound.

In this article, we propose a new mechanism for generating the DM relic abundance. We propose that DM freeze-out did not result from the gradual cooling of the cosmological plasma, but instead was triggered abruptly by a first-order cosmological phase transition (FOPT). During the transition, DM particles acquired a mass and low-momentum particles were "filtered" out of the plasma. We will see that DM filtration provides a viable production mechanism, even for DM with masses above the GK bound.

The impact of cosmological phase transitions on DM has been studied in a variety of different contexts [7]. For instance, a phase transition may alter the expansion rate of the Universe during thermal freeze-out [8–10], alter DM stability [11–13], alter DM properties during freeze-in [14, 15] (see also [16]), may produce DM non-thermally [17–20], or may produce an excess of DM over antimatter [21–25]. Freeze-out during a second order phase transition has been studied in [26], and [27] used domain walls to "sweep away" over-abundant magnetic monopoles.

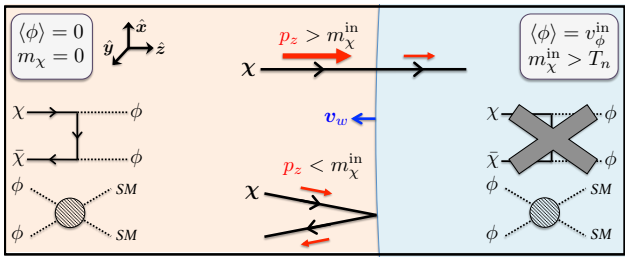

Figure 1: "Filtered DM": only DM particles χ with kinetic energy $E > m_\chi^{\rm in}$ can penetrate the bubble; slower particles are reflected. In front of the bubble wall (pink region), DM is kept in thermal equilibrium through $\chi\bar{\chi} \leftrightarrow \phi\phi$, but this reaction is put abruptly out of equilibrium at the wall where χ obtains a mass (blue region). The field ϕ remains in equilibrium throughout.

2. The mechanism. Our proposed mechanism for DM filtration during a FOPT is illustrated in Fig. 1. DM particles χ are initially massless (or relatively light) and in thermal equilibrium with SM particles and a new scalar particle ϕ. We imagine that ϕ undergoes the phase transition at temperature T_n: its thermal expectation value is initially vanishing, $\langle\phi\rangle = 0$, but jumps to a non-zero value, $\langle\phi\rangle = v_\phi^{\rm in}$, during the phase transition. FOPTs proceed through the nucleation and growth of bubbles of the new $\langle\phi\rangle = v_\phi^{\rm in}$ phase [28]. These bubbles expand and merge until the whole universe has transitioned to the new phase. At the interface of the old and new phase there is a bubble wall where $\langle\phi\rangle$ smoothly transitions from zero to $v_\phi^{\rm in}$.

We assume that $\langle\phi\rangle \neq 0$ generates a mass for the DM particles, $m_\chi^{\rm in} \propto v_\phi^{\rm in}$, so massless DM particles become massive as they cross the wall into the bubble. Energy conservation implies that a DM particle can only penetrate the bubble wall if its kinetic energy is greater than $m_\chi^{\rm in}$. Lower momentum modes are reflected by the advancing bubble walls. If $m_\chi^{\rm in} \gg T$, then only an exponentially small fraction of the DM particles will have enough kinetic energy to enter the bubbles. As DM particles enter the bubble, their interactions are put abruptly out of equilibrium, preventing their annihilation. DM particles outside the bubble in contrast will continue to interact efficiently, so that the particles reflected off the bubble walls quickly annihilate away into the thermal bath. Once the broken phase permeates the whole universe, only the particles that have entered the bubbles remain and constitute the DM observed today.

3. A toy model. To derive quantitative results, we introduce a toy model, which is also a viable theory of DM in its own right. We augment the SM by a gauge-singlet real scalar field $\phi(x)$ and a singlet Dirac spinor field $\chi(x)$. The Lagrangian defining this theory contains the terms

$$\mathscr{L} \supset -V(\phi) - y_\chi \phi \bar{\chi}\chi - \beta\,\phi^2 H^\dagger H\ , \qquad (1)$$

where $V(\phi)$ is the scalar potential, y_χ is a real Yukawa coupling, β is a real Higgs portal coupling, and $H(x)$ is the SM Higgs field. We do not assume any particular form for $V(\phi)$, only that it gives ϕ a mass m_ϕ and causes a FOPT in which ϕ acquires a non-zero vacuum expectation value $\langle 0|\phi|0\rangle = v_\phi$. Typically $v_\phi^{\rm in} \lesssim v_\phi$. For simplicity we assume that the mass of ϕ does not change appreciably during the phase transition. Note that χ enjoys a global $U(1)$ symmetry that ensures its stability.

After the phase transition, the Yukawa interaction induces a mass for DM particles, $m_\chi^{\rm in} = y_\chi v_\phi^{\rm in}$. It also allows χ to annihilate, chiefly via $\chi\bar{\chi} \to \phi\phi$. We will be interested in regimes where $m_\chi^{\rm in} \gg T_n \sim m_\phi$. We treat $v_\phi^{\rm in}/T_n$ as a free parameter, since we do not specify the form of $V(\phi)$, but we remark that large order parameters may arise from nearly conformal potentials [29–31] or models with heavy fermions (such as χ here) [32, 33].

The Higgs portal interaction [34–36] in Eq. (1) allows the hidden sector to communicate with the SM, through reactions such as $\phi\phi \leftrightarrow H^\dagger H$ if m_ϕ is above the Higgs mass, m_h, and $\phi\phi \leftrightarrow f\bar{f}$ if not. We ensure that β is large enough to thermalise ϕ and the SM at a common temperature T_n during the phase transition. At later times the Higgs portal interaction also allows ϕ particles to decay to SM particles. If $m_\phi < m_h/2 \simeq 62.5\,\text{GeV}$, the Higgs portal coupling is constrained to be $\beta \lesssim 0.007(1-4m_\phi^2/m_h^2)^{-1/4}$ [37] whereas β is almost entirely unconstrained if $m_\phi > m_h/2$.

A relatively large $m_\chi^{\rm in}$ ensures that $\chi\bar{\chi} \leftrightarrow \phi\phi$ is out of equilibrium inside the bubble. If this were not the case, χ would remain in thermal equilibrium through the phase transition and its relic abundance would later be determined by standard thermal freeze-out. We therefore require the thermally-averaged annihilation rate Γ to be smaller than the cosmological expansion rate H inside the bubble. This leads to the condition

$$\frac{m_\chi^{\rm in}}{T_n} \gtrsim 24 - \log\frac{T_n}{\text{TeV}} - \frac{3}{2}\log\frac{m_\chi^{\rm in}/T_n}{24} + 4\log y_\chi\,, \qquad (2)$$

where we have used $H = (\pi/\sqrt{90})\,g_*\,T_n^2/M_{\rm pl}$ and $\Gamma = \langle\sigma v\rangle\, n_\chi^{\rm in,eq}$, with the thermally averaged annihilation cross section $\langle\sigma v\rangle \simeq (9\,y_\chi^4\,T_n)/(64\pi\,(m_\chi^{\rm in})^3)$ [3] and the would-be equilibrium abundance $n_\chi^{\rm in,eq} = g_\chi(m_\chi^{\rm in}T_n/2\pi)^{3/2}\,e^{-m_\chi^{\rm in}/T_n}$. $g_\chi = 2$ counts the spin states, $g_* \simeq 100$ is the effective number of relativistic species, and $M_{\rm pl} \simeq 2.43\times10^{18}\,\text{GeV}$ is the reduced Planck mass.

4. Analytic estimates. We first estimate the DM relic abundance by employing a simplified description of the phase transition dynamics, treating the χ particles as they interact with the wall as if they were free particles. In other words, we assume that the thickness of the bubble wall, l_w is much smaller than the DM interaction length $l_{\rm int}$. Due to energy conservation, the mass increase of χ particles crossing the wall implies that only high-momentum particles can enter the bubble, while low-momentum ones will be reflected. After a distance $l_{\rm int}$ these reflected particles will be absorbed back into the thermal bath. In this way, low-momentum χ particles are filtered out of the plasma by the wall. Both reflected and penetrating particles transfer momentum to the bubble wall, leading to friction that limits the speed at which the wall advances, v_w [38, 39].

Using energy and transverse momentum conservation, we find that a massless χ particle that's incident on the wall with momentum $\mathbf{p} = (p_x, p_y, p_z)$ (in the plasma's rest frame) will only have sufficient energy to enter the bubble if $\gamma_w(p_z + v_w\,|\mathbf{p}|) > m_\chi^{\rm in}$ [40], where $\gamma_w = 1/\sqrt{1-{v_w}^2}$ is the wall's Lorentz factor and we have assumed the wall moves in the negative z direction. Once such a particle enters the bubble it slows down to travel with a speed $v_\chi^{\rm in} = [\,|\mathbf{p}|^2 - (m_\chi^{\rm in})^2\,]^{1/2}/m_\chi^{\rm in}$. We will be interested in non-relativistic walls, $v_w \lesssim 0.1$ because of the aforementioned friction effect. Moreover, if the wall moves relativistically, most χ particles can easily enter the bubble.

If a thermal flux of χ particles is incident on the wall, the number density $n_\chi^{\rm in}$ of χ particles that have entered the bubble is

$$n_\chi^{\rm in} = n_{\bar{\chi}}^{\rm in} = g_\chi \int \frac{{\rm d}^3\mathbf{p}}{(2\pi)^3}\,\frac{\Theta(p_z + v_w\,|\mathbf{p}| - m_\chi^{\rm in}/\gamma_w)}{e^{|\mathbf{p}|/T_n}+1}\,\frac{1}{v_\chi^{\rm in}}$$
$$\approx \frac{g_\chi(m_\chi^{\rm in}T_n)^{3/2}}{4(2\pi)^{3/2}}\,e^{-m_\chi^{\rm in}/T_n} = \frac{1}{4}n_\chi^{\rm in,eq}\,, \qquad (3)$$

where the step function Θ enforces the kinematic condition above, $n_\chi^{\rm in,eq}$ was defined below Eq. (2), and $1/v_\chi^{\rm in}$ accounts for the reduced speed of particles inside the bubble. The Boltzmann-like exponential factor is crucial in suppressing the abundance of DM inside the bubbles and therefore in setting the relic abundance.

Since $\chi\bar{\chi} \leftrightarrow \phi\phi$ is out of equilibrium inside the bubble, the χ and $\bar{\chi}$ particles that enter during the phase transition will survive until today, where they constitute the relic population of DM. The corresponding relic abundance $\Omega_{\rm DM}$ is calculated by scaling $n_\chi^{\rm in} + n_{\bar{\chi}}^{\rm in}$ with the entropy density $s = (2\pi^2/45) g_{*S} T^3$, where $g_{*S} = g_*$ at T_n and $g_{*S} = g_{*S0} \equiv 3.9$ today. After normalizing to the critical density $\rho_c = 3H_0^2 M_{\rm pl}^2$, we obtain

$$\Omega_{\rm DM} h^2 \simeq \frac{m_\chi (n_\chi^{\rm in} + n_{\bar{\chi}}^{\rm in})}{3M_{\rm pl}^2 (H_0/h)^2} \frac{g_{*S0} T_0^3}{g_{*S} T_n^3} \simeq 0.17 \left(\frac{T_n}{\rm TeV}\right) \left(\frac{m_\chi^{\rm in}/T_n}{30}\right)^{5/2} \frac{e^{-m_\chi^{\rm in}/T_n}}{e^{-30}}\,, \quad (4)$$

where $H_0 = 100\,h$ km/sec/Mpc is the Hubble constant and $T_0 \simeq 0.235\,$meV is the temperature of the cosmic microwave background today. In obtaining this estimate, we have neglected the heating of the SM bath by the annihilation of the reflected χ particles in front of wall and by the eventual decay of ϕ. This is justified because the number of SM degrees of freedom at $T_n \gtrsim$ GeV is much larger than the number of dark sector degrees of freedom. The observed DM relic abundance, $\Omega_{\rm DM}^{\rm obs} h^2 \simeq 0.12$ [41], is obtained if the DM mass increases to $m_\chi^{\rm in} \sim 30\,T_n$ inside the bubble for $T_n \sim 1\,$TeV. At higher (lower) phase transition temperatures, the required $m_\chi^{\rm in}/T_n$ becomes larger (smaller), but only logarithmically due to the exponential suppression. Comparing Eq. (4) against the standard thermal freeze-out calculation, we note that our predicted relic abundance only depends on the DM's interaction strength, y_χ, through $m_\chi^{\rm in}/T_n = y_\chi v_\chi^{\rm in}/T_n$, and consequently there is a not a one-to-one mapping from the parameters that set the relic abundance to the parameters probed, for instance, by direct detection experiments.

5. Numerical solution of Boltzmann's equation. To obtain a more accurate estimate of the relic abundance, we numerically solve the Boltzmann equations describing the χ particles near the bubble wall. A detailed discussion can be found in the Supplementary Material.

Since the scattering and diffusion length scales are small compared to the curvature scale of a typical bubble, we assume that the bubble wall is planar, and take the wall to be perpendicular to the z-axis. Since the wall experiences a significant drag force from the the scattering of χ particles, we assume a constant non-relativistic (terminal) wall speed, v_w. We choose $v_w = 0.01$ but have checked that the final relic abundance is not strongly dependent on its precise value. We approximate the mass profile of DM particles across the wall with a smoothed step-function, $m_\chi(z) = \frac{1}{2} m_\chi^{\rm in}[1 + \tanh(3z/l_w)]$. Here and in the remainder of the article we work in the wall's rest frame. We use a wall thickness $l_w = 1/(4T_n)$, but find that the final relic abundance does not depend strongly on the precise value.

Let $f_a(t, \mathbf{x}, \mathbf{p})$ be the phase space distribution functions for $a = \chi$, $\bar{\chi}$, and ϕ particles. We assume that the conserved χ–$\bar{\chi}$ asymmetry is vanishing, thus $f_{\bar{\chi}} = f_\chi$, and that ϕ remains in equilibrium throughout the phase transition, that is $f_\phi = f_\phi^{\rm eq}$ is the Bose-Einstein distribution. This is justified provided that the Higgs portal coupling β is large enough for ϕ depletion to keep up with ϕ production via $\chi\bar{\chi} \to \phi\phi$. Far in front of the wall ($z \to -\infty$), $f_\chi = f_\chi^{\rm eq}$ follows the Fermi-Dirac distribution. We adopt the ansatz,

$$f_\chi(z, \mathbf{p}) = \mathcal{A}(z, p_z) \times f_\chi^{\rm eq}(z, \mathbf{p})\,, \quad (5)$$

as motivated in the Supplementary Material. The distribution f_χ in the vicinity of the bubble wall can then be described by the Boltzmann equation

$$\left[\left(\frac{p_z}{m_\chi}\frac{\partial}{\partial z} - \left(\frac{\partial m_\chi}{\partial z}\right)\frac{\partial}{\partial p_z} - \left(\frac{\partial m_\chi}{\partial z}\right)\frac{v_w}{T_n}\right)\mathcal{A}(z, p_z)\right] \frac{g_\chi m_\chi T_n}{2\pi} \exp\left[\frac{v_w p_z - \sqrt{m_\chi^2 + (p_z)^2}}{T_n}\right] = g_\chi \int \frac{{\rm d}p_x\,{\rm d}p_y}{(2\pi)^2}\,\mathbf{C}[f_\chi]\,. \quad (6)$$

The right hand side includes the collision terms for the processes $\chi\bar{\chi} \to \phi\phi$, $\chi\phi \to \chi\phi$, $\chi\chi \to \chi\chi$ and $\chi\bar{\chi} \to \chi\bar{\chi}$. Note that we have integrated over p_x and p_y. Integrating over p_z will then yield the number density at a position z.

We are interested in solutions of Eq. (6) that obey the boundary conditions

$$\lim_{\substack{z\to-\infty \\ p_z>0}} \mathcal{A} \to 1 \quad \text{and} \quad \lim_{z\to\infty} \mathcal{A}(p_z) = \lim_{z\to\infty} \mathcal{A}(-p_z)\,. \quad (7)$$

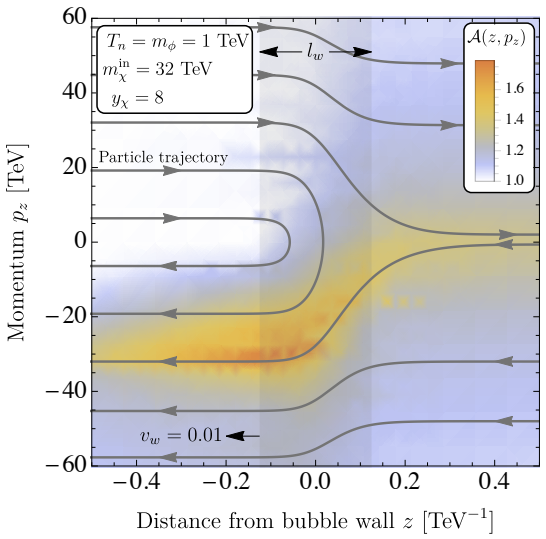

Figure 2: The enhancement factor $\mathcal{A}(z, p_z)$ in the neighbourhood of the bubble wall (opaque vertical band). Contours with arrows indicate possible particle trajectories in this two-dimensional phase space. For the chosen parameter values, we recover the observed relic abundance.

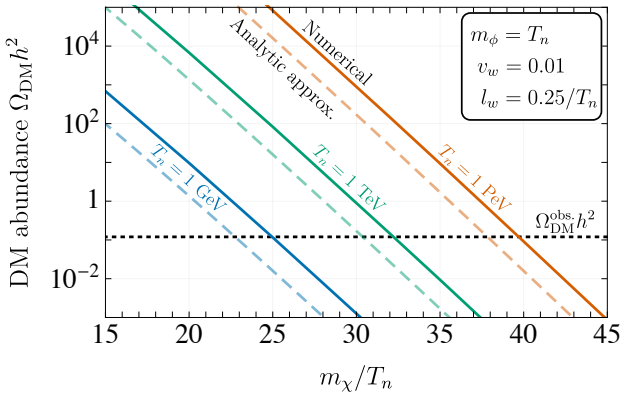

Figure 3: The DM relic abundance as a function of the phase transition's temperature T_n and the χ particle's mass m_χ, where we assume $m_\chi \approx m_\chi^{\rm in}$. The solid lines are calculated by numerically solving Boltzmann's equation while the dashed lines show the analytic approximation, Eq. (4).

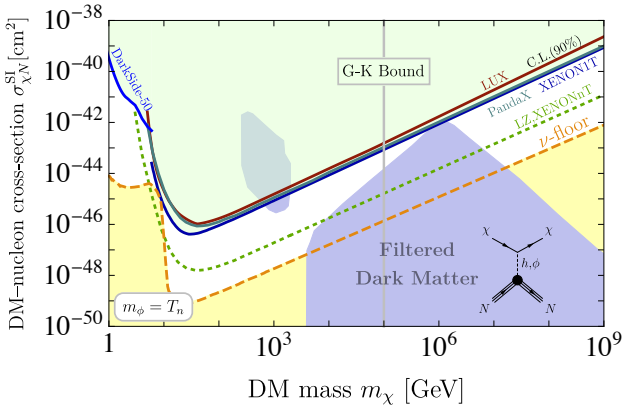

Figure 4: The predicted spin-independent DM–nucleon scattering cross-section (purple shaded region) in comparison with various experimental exclusions limits (green shaded) [42–45], projected sensitivities of future experiments (green dashed) [46], and the neutrino floor (yellow shaded). Note that viable models of filtered DM are obtained even at large values of the DM mass, above the Griest–Kamionkowski bound, $m_\chi \sim 100\,$TeV.

The first condition enforces an equilibrium phase space distribution for particles that have not yet interacted with the bubble wall, while the second condition is based on the assumption that at a large positive z the other side of the bubble is advancing with similar dynamics. We solve Eqs. (6) and (7) numerically using the method of characteristics, where the 2-dimensional partial differential equation is re-written as an infinite set of uncoupled ordinary differential equations. Each equation corresponds to a possible particle trajectory in the two-dimensional phase space spanned by z and p_z, in the absence of collisions. A typical solution for $\mathcal{A}(z, p_z)$ is shown in Fig. 2, along with some of the aforementioned particle trajectories. Particles incident on the wall begin in equilibrium (upper-left quadrant), so $\mathcal{A}(z, p_z) \approx 1$. Those that started with a momentum larger than $m_\chi^{\rm in}$ enter the bubble (upper-right), with $\mathcal{A} \approx 1.2$. That is, with an abundance only slightly larger than the strongly Boltzmann-suppressed $f_\chi^{\rm eq}(z, \mathbf{p})$. Particles that started with a momentum lower than $m_\chi^{\rm in}$ are reflected by the wall (mid-left). Particles that come from $z \to \infty$ (lower-right) receive a boost in momentum as they leave the bubble. These boosted particles and the reflected particles lead to an overdensity, which annihilates into the thermal bath as the particles travel away from the wall (bottom-left).

We then integrate over p_z deep inside the bubble to find the resulting DM relic abundance, and present our results in Fig. 3. We assume $m_\chi \approx m_\chi^{\rm in}$, implying a negligible change in the χ particle's mass between the phase transition and today. The observed relic abundance is obtained for $m_\chi/T_n \approx (25, 32, 40)$ and $T_n = (1\,\text{GeV}, 1\,\text{TeV}, 1\,\text{PeV})$, respectively. These parameters are consistent with the out-of-equilibrium condition Eq. (2) provided that $y_\chi < (0.2, 8, 4\pi)$, respectively. The exponential sensitivity to $m_\chi/T_n \approx m_\chi^{\rm in}/T_n$ is clearly visible. Comparing the numerical result with the analytical estimate from Eq. (4), we find good agreement of the parametric dependences on T_n and $m_\chi^{\rm in}/T_n$, and the overall amplitude differs by a factor of ~ 5.

6. Current and future probes. Filtered DM is amenable to many of the same tests as thermal relic (WIMP) DM. Direct detection of χ particles is mediated,

in this toy model, by a t-channel exchange of ϕ particles and Higgs bosons (h) so the rate is suppressed by the tiny ϕ–h mixing [47]. In Fig. 4 the purple region shows the range of spin-independent χ–nucleon scattering cross-sections $\sigma^{\rm SI}_{\chi N}$. We impose the conditions that $\Omega_\chi = \Omega^{\rm obs.}_{\rm DM}$, that couplings remain perturbative ($y_\chi, \beta < 4\pi$), that χ is in equilibrium outside the bubble (imposes a lower bound on y_χ) and out of equilibrium inside the bubble, Eq. (2), and that ϕ is in equilibrium throughout the phase transition (imposes a lower bound on β). At $m_\chi \ll 100\,\text{GeV}$, the dark sector no longer stays in equilibrium outside the bubble because $\phi\phi$ annihilation is suppressed by the Higgs mass and small SM Yukawa couplings. Around masses of several TeV, the value of β required to keep ϕ in equilibrium grows, making it impossible to obtain the correct Higgs mass from the scalar mass matrix. At even larger m_χ, this problem disappears as new ϕ annihilation channels open up. We see that there is a large region of viable parameter space at masses above the Griest–Kamionkowski bound [5, 6].

At current and future collider experiments, filtered DM can be tested through precision measurements of the Higgs boson's couplings to other SM particles [48–51]. These measurements already constrain the ϕ–h mixing for sub-TeV masses [52, 53].

Annihilations of χ and $\bar{\chi}$ to SM particles in the Milky Way's DM halo provide another avenue to indirectly detect filtered DM. For instance, decays of the annihilation products may be a source of PeV-scale neutrinos. Detection prospects are however hampered by p-wave suppressed annihilation cross-sections.

The bubble dynamics during the FOPT produce a stochastic background of gravitational waves [54]. The frequency of this gravitational wave radiation is tied to the mass scale of filtered DM. However, we expect the signal strength to be suppressed by the small bubble wall speed and a dedicated analysis is required to determine if this signal is within reach of next-generation gravitational wave telescopes, e.g., LISA [55].

7. Discussion and Conclusions. In summary, we have shown that dark matter freeze out can be triggered by a first order cosmological phase transition, which effectively *filters* low-momentum particles out of the phase space distribution. Perhaps most notably, dark matter filtration is viable mechanism of dark matter generation even for dark matter masses above the Griest–Kamionkowski bound. Potential signatures include direct, indirect, and collider probes of WIMP dark matter as well as a stochastic gravitational wave signal.

Acknowledgments. The authors would like to thank Andrea Thamm for comments on the manuscript. The authors would also like to express a special thanks to the Mainz Institute for Theoretical Physics (MITP) for its hospitality and support during key parts of the collaboration. M.J.B. was supported by the Australian Research Council and by the Swiss National Science Foundation (SNF) under contract 200021-159720. J.K. has been partially supported by the European Research Council (ERC) under the European Union's Horizon 2020 research and innovation program (grant agreement No. 637506, "νDirections") and by the German Research Foundation (DFG) under grant No. KO 4820/4-1. A.J.L. was supported in part by the US Department of Energy under grant DE-SC0007859.

* Electronic address: michael.baker@unimelb.edu.au
† Electronic address: jkopp@cern.ch
‡ Electronic address: andrewjlong@rice.edu

[1] G. Bertone and D. Hooper, *History of dark matter*, *Rev. Mod. Phys.* **90** (2018), no. 4 045002, [arXiv:1605.04909].
[2] M. Srednicki, R. Watkins, and K. A. Olive, *Calculations of Relic Densities in the Early Universe*, *Nucl. Phys.* **B310** (1988) 693. [,247(1988)].
[3] P. Gondolo and G. Gelmini, *Cosmic abundances of stable particles: Improved analysis*, *Nucl. Phys.* **B360** (1991) 145–179.
[4] K. Griest and D. Seckel, *Three exceptions in the calculation of relic abundances*, *Phys. Rev.* **D43** (1991) 3191–3203.
[5] K. Griest and M. Kamionkowski, *Unitarity Limits on the Mass and Radius of Dark Matter Particles*, *Phys. Rev. Lett.* **64** (1990) 615.
[6] I. Baldes and K. Petraki, *Asymmetric thermal-relic dark matter: Sommerfeld-enhanced freeze-out, annihilation signals and unitarity bounds*, *JCAP* **1709** (2017), no. 09 028, [arXiv:1703.00478].
[7] D. N. Schramm, *Phase Transitions and Dark Matter Problems*, *Nucl. Phys.* **B252** (1985) 53–71.
[8] E. W. Kolb and S. Wolfram, *Spontaneous Symmetry Breaking and the Expansion Rate of the Early Universe*, *Astrophys. J.* **239** (1980) 428.
[9] D. Chung, A. Long, and L.-T. Wang, *Probing the Cosmological Constant and Phase Transitions with Dark Matter*, *Phys. Rev.* **D84** (2011) 043523, [arXiv:1104.5034].
[10] D. J. H. Chung and A. J. Long, *Cosmological Constant, Dark Matter, and Electroweak Phase Transition*, *Phys. Rev.* **D84** (2011) 103513, [arXiv:1108.5193].
[11] M. J. Baker and J. Kopp, *Dark Matter Decay between Phase Transitions at the Weak Scale*, *Phys. Rev. Lett.* **119** (2017), no. 6 061801, [arXiv:1608.07578].
[12] M. J. Baker, *Dark matter models beyond the WIMP paradigm*, *Nuovo Cim.* **C40** (2017), no. 5 163.
[13] M. J. Baker and L. Mittnacht, *Variations on the Vev Flip-Flop: Instantaneous Freeze-out and Decaying Dark Matter*, *JHEP* **05** (2019) 070, [arXiv:1811.03101].
[14] M. J. Baker, M. Breitbach, J. Kopp, and L. Mittnacht, *Dynamic Freeze-In: Impact of Thermal Masses and Cosmological Phase Transitions on Dark Matter Production*, *JHEP* **03** (2018) 114, [arXiv:1712.03962].
[15] L. Bian and Y.-L. Tang, *Thermally modified sterile neutrino portal dark matter and gravitational waves from phase transition: The Freeze-in case*, *JHEP* **12** (2018) 006, [arXiv:1810.03172].

[16] T. Cohen, D. E. Morrissey, and A. Pierce, *Changes in Dark Matter Properties After Freeze-Out*, *Phys. Rev.* **D78** (2008) 111701, [arXiv:0808.3994].

[17] E. Witten, *Cosmic Separation of Phases*, *Phys. Rev.* **D30** (1984) 272–285.

[18] A. Falkowski and J. M. No, *Non-thermal Dark Matter Production from the Electroweak Phase Transition: Multi-TeV WIMPs and 'Baby-Zillas'*, *JHEP* **02** (2013) 034, [arXiv:1211.5615].

[19] F. P. Huang and C. S. Li, *Probing the baryogenesis and dark matter relaxed in phase transition by gravitational waves and colliders*, *Phys. Rev.* **D96** (2017), no. 9 095028, [arXiv:1709.09691].

[20] Y. Bai, A. J. Long, and S. Lu, *Dark Quark Nuggets*, *Phys. Rev.* **D99** (2019), no. 5 055047, [arXiv:1810.04360].

[21] S. Dodelson, B. R. Greene, and L. M. Widrow, *Inverse phase transitions: Does baryogenesis lead to dark matter?*, in *15th Johns Hopkins Workshop on Current Problems in Particle Theory: Particle Physics from Underground to Heaven Baltimore, Maryland, August 26-28, 1991*, pp. 391–402, 1992.

[22] K. Petraki, M. Trodden, and R. R. Volkas, *Visible and dark matter from a first-order phase transition in a baryon-symmetric universe*, *JCAP* **1202** (2012) 044, [arXiv:1111.4786].

[23] I. Baldes, *Gravitational waves from the asymmetric-dark-matter generating phase transition*, *JCAP* **1705** (2017), no. 05 028, [arXiv:1702.02117].

[24] P.-H. Gu, *Cosmic matter from dark electroweak phase transition with neutrino mass generation*, *Phys. Rev.* **D96** (2017), no. 5 055038, [arXiv:1705.05189].

[25] E. Hall, T. Konstandin, R. McGehee, and H. Murayama, *Asymmetric Matters from a Dark First-Order Phase Transition*, arXiv:1911.12342.

[26] S. Dimopoulos, R. Esmailzadeh, L. J. Hall, and N. Tetradis, *Electroweak phase transition and dark matter abundance*, *Phys. Lett.* **B247** (1990) 601–606.

[27] G. R. Dvali, H. Liu, and T. Vachaspati, *Sweeping away the monopole problem*, *Phys. Rev. Lett.* **80** (1998) 2281–2284, [hep-ph/9710301].

[28] A. D. Linde, *Decay of the False Vacuum at Finite Temperature*, *Nucl. Phys.* **B216** (1983) 421. [Erratum: Nucl. Phys.B223,544(1983)].

[29] P. Creminelli, A. Nicolis, and R. Rattazzi, *Holography and the electroweak phase transition*, *JHEP* **03** (2002) 051, [hep-th/0107141].

[30] G. Nardini, M. Quiros, and A. Wulzer, *A Confining Strong First-Order Electroweak Phase Transition*, *JHEP* **09** (2007) 077, [arXiv:0706.3388].

[31] T. Konstandin and G. Servant, *Cosmological Consequences of Nearly Conformal Dynamics at the TeV scale*, *JCAP* **1112** (2011) 009, [arXiv:1104.4791].

[32] M. Carena, A. Megevand, M. Quiros, and C. E. M. Wagner, *Electroweak baryogenesis and new TeV fermions*, *Nucl. Phys.* **B716** (2005) 319–351, [hep-ph/0410352].

[33] A. Angelescu and P. Huang, *Multistep Strongly First Order Phase Transitions from New Fermions at the TeV Scale*, *Phys. Rev.* **D99** (2019), no. 5 055023, [arXiv:1812.08293].

[34] V. Silveira and A. Zee, *SCALAR PHANTOMS*, *Phys. Lett.* **161B** (1985) 136–140.

[35] C. P. Burgess, M. Pospelov, and T. ter Veldhuis, *The Minimal model of nonbaryonic dark matter: A Singlet scalar*, *Nucl. Phys.* **B619** (2001) 709–728, [hep-ph/0011335].

[36] B. Patt and F. Wilczek, *Higgs-field portal into hidden sectors*, hep-ph/0605188.

[37] **CMS** Collaboration, A. M. Sirunyan et al., *Search for invisible decays of a Higgs boson produced through vector boson fusion in proton-proton collisions at* $\sqrt{s} =$ *13 TeV*, *Phys. Lett.* **B793** (2019) 520–551, [arXiv:1809.05937].

[38] G. D. Moore and T. Prokopec, *Bubble wall velocity in a first order electroweak phase transition*, *Phys. Rev. Lett.* **75** (1995) 777–780, [hep-ph/9503296].

[39] G. D. Moore and T. Prokopec, *How fast can the wall move? A Study of the electroweak phase transition dynamics*, *Phys. Rev.* **D52** (1995) 7182–7204, [hep-ph/9506475].

[40] D. Bodeker and G. D. Moore, *Can electroweak bubble walls run away?*, *JCAP* **0905** (2009) 009, [arXiv:0903.4099].

[41] **Planck** Collaboration, N. Aghanim et al., *Planck 2018 results. VI. Cosmological parameters*, arXiv:1807.06209.

[42] **LUX** Collaboration, D. S. Akerib et al., *Results from a search for dark matter in the complete LUX exposure*, *Phys. Rev. Lett.* **118** (2017), no. 2 021303, [arXiv:1608.07648].

[43] **PandaX-II** Collaboration, X. Cui et al., *Dark Matter Results From 54-Ton-Day Exposure of PandaX-II Experiment*, *Phys. Rev. Lett.* **119** (2017), no. 18 181302, [arXiv:1708.06917].

[44] **XENON** Collaboration, E. Aprile et al., *Dark Matter Search Results from a One Ton-Year Exposure of XENON1T*, *Phys. Rev. Lett.* **121** (2018), no. 11 111302, [arXiv:1805.12562].

[45] **DarkSide** Collaboration, P. Agnes et al., *Low-Mass Dark Matter Search with the DarkSide-50 Experiment*, *Phys. Rev. Lett.* **121** (2018), no. 8 081307, [arXiv:1802.06994].

[46] **LUX-ZEPLIN** Collaboration, D. S. Akerib et al., *Projected WIMP Sensitivity of the LUX-ZEPLIN (LZ) Dark Matter Experiment*, arXiv:1802.06039.

[47] S. Matsumoto, Y.-L. S. Tsai, and P.-Y. Tseng, *Light Fermionic WIMP Dark Matter with Light Scalar Mediator*, *JHEP* **07** (2019) 050, [arXiv:1811.03292].

[48] K. Fujii et al., *Physics Case for the 250 GeV Stage of the International Linear Collider*, arXiv:1710.07621.

[49] **CEPC Study Group** Collaboration, M. Dong et al., *CEPC Conceptual Design Report: Volume 2 - Physics & Detector*, arXiv:1811.10545.

[50] **FCC** Collaboration, A. Abada et al., *FCC Physics Opportunities*, *Eur. Phys. J.* **C79** (2019), no. 6 474.

[51] **HL/HE WG2 group** Collaboration, M. Cepeda et al., *Higgs Physics at the HL-LHC and HE-LHC*, arXiv:1902.00134.

[52] **ATLAS, CMS** Collaboration, G. Aad et al., *Measurements of the Higgs boson production and decay rates and constraints on its couplings from a combined ATLAS and CMS analysis of the LHC pp collision data at* $\sqrt{s} = 7$ *and 8 TeV*, *JHEP* **08** (2016) 045, [arXiv:1606.02266].

[53] M. Carena, Z. Liu, and M. Riembau, *Probing the electroweak phase transition via enhanced di-Higgs boson production*, *Phys. Rev.* **D97** (2018), no. 9 095032,

[arXiv:1801.00794].

[54] M. Kamionkowski, A. Kosowsky, and M. S. Turner, *Gravitational radiation from first order phase transitions*, *Phys. Rev.* **D49** (1994) 2837–2851, [astro-ph/9310044].

[55] C. Caprini et al., *Detecting gravitational waves from cosmological phase transitions with LISA: an update*, arXiv:1910.13125.

Filtered Dark Matter at a First Order Phase Transition

Supplementary Material

Michael J. Baker, Joachim Kopp, and Andrew J. Long

DERIVATION OF THE BOLTZMANN EQUATIONS

Here we present a derivation and further discussion of the Boltzmann equation, Eq. (6) in the main text. We start from the general Boltzmann equation for the phase space distribution of χ particles, f_χ,

$$\mathbf{L}[f_\chi] = \mathbf{C}[f_\chi]\,. \tag{S1}$$

Here, $\mathbf{L}$ is the Liouville operator, which describes the evolution of f_χ in the absence of particle scattering, and $\mathbf{C}$ is a collision term, which accounts for any particle number changing processes as well as elastic scattering.

Before discussing these terms in more detail, we motivate the ansatz that we will use, Eq. (5) in the main text. We start with the Maxwell-Boltzmann approximation for the equilibrium distribution function, which in the plasma frame is

$$f_\chi^{\rm eq} \approx \exp\left(\frac{\mu}{T}\right)\exp\left(-\frac{E^p}{T}\right)\,, \tag{S2}$$

where μ is the chemical potential, the energy $E^p = \sqrt{m(z^p,t^p)^2 + (\mathbf{p}^p)^2}$, and z^p, t^p and $\mathbf{p}^p$ are the position perpendicular to the wall, the time coordinate and the 3-momentum in the plasma frame. The Maxwell-Boltzmann approximation is very good in the non-relativistic regime and gives an error of $\approx 5\%$ for both fermions and bosons in the ultra-relativistic regime where the mass is negligible and the energy $\approx 3T$. Since in the rest frame of the wall the mass of χ is a function of the position perpendicular to the wall, z^w, alone, it is natural to work in that frame. The energy of a particle in the wall frame E^w is related to the energy in the plasma frame by

$$E^p = \gamma_w\left(E^w - v_w p_z^w\right)\,, \tag{S3}$$

where $\boldsymbol{v}_w = -v_w\,\hat{\boldsymbol{z}}$ is the bubble wall velocity (in natural units) and $\gamma_w = 1/\sqrt{1-{v_w}^2}$ is the corresponding Lorentz factor. We take the wall to be moving in the negative z direction, so the wall speed v_w is positive. We expect interactions with the wall to cause deviations from equilibrium. In order to describe these deviations in front of the wall it is essential to retain the dependence on z^w and p_z^w (the momentum perpendicular to the wall in the wall frame). For simplicity, we will, however, assume that the pre-factor $\mathcal{A}$ which describes the deviation from equilibrium and also absorbs the chemical potential term, does not depend on p_x or p_y. This motivates the ansatz

$$f_\chi = \mathcal{A}(z^w, p_z^w)\exp\left(-\frac{E^p}{T}\right)\,. \tag{S4}$$

While this is related to the fluid ansatz [39] , we take the temperature to be homogeneous, but introduce dependence on p_z^w. Although χ is not in equilibrium inside the bubble, we see from Eq. (3) that we expect an order one deviation from equilibrium inside the bubble, so $\mathcal{A}(z^w, p_z^w)$ should not deviate dramatically from one.

The Liouville Operator

The Liouville operator is the total time derivative of the phase space distribution function $f = f(t, \mathbf{x}(t), \mathbf{p}(t))$. In the wall frame, it is given by

$$\mathbf{L}[f_\chi] = \frac{df_\chi}{dt^w} = \frac{\partial f_\chi}{\partial t^w} + \frac{\partial \mathbf{x}^w}{\partial t^w}\frac{\partial f_\chi}{\partial \mathbf{x}^w} + \frac{\partial \mathbf{p}^w}{\partial t^w}\frac{\partial f_\chi}{\partial \mathbf{p}^w}\,. \tag{S5}$$

We assume that the system has reached a steady-state ($\partial f_\chi/\partial t^w = 0$) in the wall frame. Since the system is translation invariant in x and y, we can simplify $\mathbf{L}[f_\chi]$ considerably:

$$\mathbf{L}[f_\chi] = \frac{p_z^w}{E^w}\frac{\partial f_\chi}{\partial z^w} + \frac{\partial p_z^w}{\partial t^w}\frac{\partial f_\chi}{\partial p_z^w}\,, \tag{S6}$$

where we have written the velocity $\partial z^w/\partial t^w$ as p_z^w/E^w. The factor $\partial p_z^w/\partial t^w$ can be interpreted as the semi-classical force acting on the particle as it traverses the wall. Since $E^2 = \mathbf{p}_\perp^2 + p_z^2 + m^2$ and since the particle energy and the transverse momentum $\mathbf{p}_\perp$ are conserved in the wall frame we can write

$$\begin{aligned}\frac{\partial p_z^w}{\partial t} &= \frac{\partial(\mathrm{sgn}[p_z^w]\sqrt{(E^w)^2 - p_\perp^2 - m(z^w)^2})}{\partial t} \\ &= -\frac{m(z^w)}{p_z^w}\frac{\partial z^w}{\partial t^w}\frac{\partial m(z^w)}{\partial z^w} \\ &= -\frac{m(z^w)}{E^w}\frac{\partial m(z^w)}{\partial z^w}\,.\end{aligned} \tag{S7}$$

We then have

$$\mathbf{L}[f_\chi] = \frac{p_z^w}{E^w}\frac{\partial f_\chi}{\partial z^w} - \frac{m(z^w)}{E^w}\frac{\partial m}{\partial z^w}\frac{\partial f_\chi}{\partial p_z^w}\,. \tag{S8}$$

We now integrate over the transverse momentum components p_x and p_y and multiply by the number of spin states, $g_\chi = 2$, giving

$$g_\chi\int\frac{dp_x dp_y}{(2\pi)^2}\mathbf{L}[f_\chi] = g_\chi\int\frac{dp_x dp_y}{(2\pi)^2}\frac{p_z^w}{E^w}\frac{\partial f_\chi}{\partial z^w} - g_\chi\left(\frac{\partial m}{\partial z^w}\right)\int\frac{dp_x dp_y}{(2\pi)^2}\frac{m(z^w)}{E^w}\frac{\partial f_\chi}{\partial p_z^w}\,. \tag{S9}$$

Everything that we have done so far has been analytic and exact. We now introduce the ansatz from Eq. (S4):

$$\begin{aligned}g_\chi\int\frac{dp_x dp_y}{(2\pi)^2}\mathbf{L}[f_\chi] =\, & g_\chi\left(\frac{\partial}{\partial z^w}\mathcal{A}(z^w,p_z^w)\right)\int\frac{dp_x dp_y}{(2\pi)^2}\frac{p_z^w}{E^w}f_\chi^{\mathrm{eq}} \\ & + g_\chi\mathcal{A}(z^w,p_z^w)\int\frac{dp_x dp_y}{(2\pi)^2}\frac{p_z^w}{E^w}\left(\frac{\partial}{\partial z^w}f_\chi^{\mathrm{eq}}\right) \\ & - g_\chi\left(\frac{\partial m}{\partial z^w}\right)\left(\frac{\partial}{\partial p_z^w}\mathcal{A}(z^w,p_z^w)\right)\int\frac{dp_x dp_y}{(2\pi)^2}\frac{m(z^w)}{E^w}f_\chi^{\mathrm{eq}} \\ & - g_\chi\left(\frac{\partial m}{\partial z^w}\right)\mathcal{A}(z^w,p_z^w)\int\frac{dp_x dp_y}{(2\pi)^2}\frac{m(z^w)}{E^w}\left(\frac{\partial}{\partial p_z^w}f_\chi^{\mathrm{eq}}\right).\end{aligned} \tag{S10}$$

Using the Maxwell-Boltzmann approximation for f_χ then gives

$$\begin{aligned}g_\chi\int\frac{dp_x dp_y}{(2\pi)^2}\mathbf{L}[f_\chi] \approx\, & g_\chi\left(\frac{\partial}{\partial z^w}\mathcal{A}(z^w,p_z^w)\right)\int\frac{dp_x dp_y}{(2\pi)^2}\frac{p_z^w}{\sqrt{m^2+p_x^2+p_y^2+(p_z^w)^2}}\,e^{-E^p/T} \\ & + g_\chi\mathcal{A}(z^w,p_z^w)\int\frac{dp_x dp_y}{(2\pi)^2}\frac{p_z^w}{\sqrt{m^2+p_x^2+p_y^2+(p_z^w)^2}}\left(\frac{\partial}{\partial z^w}e^{-E^p/T}\right) \\ & - g_\chi\left(\frac{\partial m}{\partial z^w}\right)\left(\frac{\partial}{\partial p_z^w}\mathcal{A}(z^w,p_z^w)\right)\int\frac{dp_x dp_y}{(2\pi)^2}\frac{m}{\sqrt{m^2+p_x^2+p_y^2+(p_z^w)^2}}e^{-E^p/T} \\ & - g_\chi\left(\frac{\partial m}{\partial z^w}\right)\mathcal{A}(z^w,p_z^w)\int\frac{dp_x dp_y}{(2\pi)^2}\frac{m}{\sqrt{m^2+p_x^2+p_y^2+(p_z^w)^2}}\left(\frac{\partial}{\partial p_z^w}e^{-E^p/T}\right) \\ =\, & \left[\left(\frac{p_z^w}{m_\chi}\frac{\partial}{\partial z^w} - \left(\frac{\partial m_\chi}{\partial z^w}\right)\frac{\partial}{\partial p_z^w} - \left(\frac{\partial m_\chi}{\partial z^w}\right)\frac{v_w}{T}\right)\mathcal{A}(z^w,p_z^w)\right]\frac{g_\chi m_\chi T}{2\pi}e^{\left(v_w p_z^w - \sqrt{m_\chi^2+(p_z^w)^2}\right)/T}\,.\end{aligned} \tag{S11}$$

Here we have used that $E^p \simeq E^w - v_w p_z^w$, which is reasonable for non-relativistic wall velocities. Since the final term in Eq. (S11) is proportional to the wall velocity, v_w, it is important to keep the wall velocity in the Liouville operator, even when dropping it elsewhere.

The Collision Term

We now turn to the collision term, $\mathbf{C}[f_\chi]$, which we evaluate in the plasma frame, only transforming to the wall frame at the end. We consider the process $\chi(p^p) + \bar{\chi}(q^p) \to \phi(k^p) + \phi(l^p)$, where the quantities in parentheses denote the momenta of the particles. The collision terms for the other processes, $\chi\phi \to \chi\phi$, $\chi\chi \to \chi\chi$ and $\chi\bar{\chi} \to \chi\bar{\chi}$, can be derived by trivial replacements. Integrating over p_x and p_y and multiplying by the number of spin states, $g_\chi = 2$, the collision term is

$$g_\chi \int \frac{dp_x dp_y}{(2\pi)^2} \mathbf{C}[f_\chi] = \sum_{\text{spins}} \int \frac{dp_x dp_y}{(2\pi)^2}\, d\Pi_{q^p}\, d\Pi_{k^p}\, d\Pi_{l^p}\, \frac{(2\pi)^4}{2E_p^p} \delta^{(4)}(p^p + q^p - k^p - l^p) |\mathcal{M}|^2 \cdot \left[f_{\chi_p} f_{\bar{\chi}_q} (1 \pm f_{\phi_k})(1 \pm f_{\phi_l}) - f_{\phi_k} f_{\phi_l} (1 \pm f_{\chi_p})(1 \pm f_{\bar{\chi}_q}) \right], \tag{S12}$$

where $\mathcal{M}$ is the CP-invariant matrix element, and we have used the shorthand notation $E_p^p = [(\mathbf{p}^p)^2 + m_\chi^2]^2$, $d\Pi_{q^p} \equiv d^3q^p/[2E_q^p\,(2\pi)^3]$, and $f_{\chi_p} \equiv f_\chi(t^p, \mathbf{x}^p, \mathbf{p}^p)$, with $\chi_p \equiv \chi(p)$. Analogous definitions are used for the other momenta and distribution functions.

We neglect Pauli blocking and Bose enhancement for all species by setting $1 \pm f \approx 1$, and we assume that all species except for the initial DM particle $\chi(p)$ are in equilibrium. For ϕ, this is always true in the parameter region of interest to us; for χ, our numerical results show that χ does not deviate from equilibrium by more than an $\mathcal{O}(1)$ factor, so the equilibrium approximation is fairly accurate for any other χ particles in the process. Since detailed balance holds for each momentum mode independently, $f_{\phi_k}^{\text{eq}} f_{\phi_l}^{\text{eq}} = f_{\chi_p}^{\text{eq}} f_{\bar{\chi}_q}^{\text{eq}}$. Equation (S12) thus simplifies to

$$g_\chi \int \frac{dp_x dp_y}{(2\pi)^2} \mathbf{C}[f_\chi] = \sum_{\text{spins}} \int \frac{dp_x dp_y}{(2\pi)^2} d\Pi_{q^p}\, d\Pi_{k^p}\, d\Pi_{l^p}\, \frac{(2\pi)^4}{2E_p^p} \delta^{(4)}(p^p + q^p - k^p - l^p) |\mathcal{M}|^2 \left[f_{\chi_p} f_{\bar{\chi}_q}^{\text{eq}} - f_{\chi_p}^{\text{eq}} f_{\bar{\chi}_q}^{\text{eq}} \right]. \tag{S13}$$

We can now integrate over k and l to obtain

$$\begin{aligned} g_\chi \int \frac{dp_x dp_y}{(2\pi)^2} \mathbf{C}[f_\chi] &= g_\chi g_{\bar{\chi}} \int \frac{dp_x dp_y}{(2\pi)^2 2E_p^p}\, d\Pi_{q^p}\, 4F \sigma_{\chi\bar{\chi}\to\phi\phi} \left[f_{\chi_p} f_{\bar{\chi}_q}^{\text{eq}} - f_{\chi_p}^{\text{eq}} f_{\bar{\chi}_q}^{\text{eq}} \right] \\ &= g_\chi g_{\bar{\chi}} \left[\mathcal{A}(z^w, p_z^w) - 1 \right] \int \frac{dp_x dp_y}{(2\pi)^2 2E_p^p}\, d\Pi_{q^p}\, 4F \sigma_{\chi\bar{\chi}\to\phi\phi} f_{\chi_p}^{\text{eq}} f_{\bar{\chi}_q}^{\text{eq}}, \end{aligned} \tag{S14}$$

where we have used the ansatz in Eq. (S4), $\sigma_{\chi\bar{\chi}\to\phi\phi}$ is the relevant spin-averaged cross-section, and where

$$F = \frac{1}{2}\sqrt{(s - m_\chi^2 - m_{\bar{\chi}}^2)^2 - 4 m_\chi^2 m_{\bar{\chi}}^2}\,. \tag{S15}$$

Although in principle we should replace E^p in the equilibrium distribution functions with $(E^w - v_w p_z^w)$, the impact of v_w is negligible in the collision term and we simply replace E^p with E^w. Making the Maxwell-Boltzmann approximation for f^{eq} then lets us perform the remaining integrals numerically reasonably quickly.

SOLVING THE BOLTZMANN EQUATIONS

We are now ready to solve the Boltzmann equation, Eq. (6), with the Liouville operator on the left-hand side given by Eq. (S11), and the collision terms on the right-hand side given by Eq. (S14), and similar terms for the other processes. This equation is a partial differential equation (PDE) of the form

$$a(z^w, p_z^w) \frac{\partial \mathcal{A}}{\partial z^w} + b(z^w, p_z^w) \frac{\partial \mathcal{A}}{\partial p_z^w} = c(\mathcal{A}, z^w, p_z^w)\,. \tag{S16}$$

PDEs of this form can be reduced to an infinite set of uncoupled ordinary differential equations (ODEs) using the method of characteristics. For any given starting point, a curve on the (z^w, p_z^w) plane can be defined via

$$\frac{dz^w(\lambda)}{d\lambda} = a(z^w, p_z^w)\,, \qquad \frac{dp_z^w(\lambda)}{d\lambda} = b(z^w, p_z^w)\,, \tag{S17}$$

where λ parameterises the curve. The solution to the PDE along each curve can then be found by integrating the ODE

$$\frac{d\mathcal{A}\big(z^w(\lambda), p_z^w(\lambda)\big)}{d\lambda} = c\big(\mathcal{A}(\lambda), z^w(\lambda), p_z^w(\lambda)\big)\,. \tag{S18}$$

To see this, note that

$$\frac{d\mathcal{A}}{d\lambda} = \frac{\partial\mathcal{A}}{\partial z^w}\frac{dz^w}{d\lambda} + \frac{\partial\mathcal{A}}{\partial p_z^w}\frac{dp_z^w}{d\lambda} = a(z^w, p_z^w)\frac{\partial\mathcal{A}}{\partial z^w} + b(z^w, p_z^w)\frac{\partial\mathcal{A}}{\partial p_z^w} = c(\mathcal{A}, z^w, p_z^w)\,. \tag{S19}$$

Numerically, the full solution to the PDE on the plane can be found by interpolating between solutions along several curves which span the region of interest. In Fig. 2 we show some of these curves. Physically, in the absence of collisions a particle with a given initial position and momentum, z^w and p_z^w, will travel along these curves in phase space as time passes. We see that particles starting outside the bubble and travelling towards the bubble wall ($z^w \ll -l_w$, $p_z^w > 0$) are either reflected from the bubble wall if $p_z^w \lesssim m_\chi^{\rm in}$, or penetrate the bubble wall if $p_z^w \gtrsim m_\chi^{\rm in}$. This is due to conservation of energy. Particles originating inside the bubble receive a boost of momentum as they leave the bubble.

The boundary conditions for the PDE become initial conditions for the ODEs. For particles outside the bubble which are approaching the bubble ($z^w \ll -l_w$, $p_z^w > 0$) we set $\mathcal{A} = 1$, so the abundance is equal to the equilibrium abundance. This assumes that χ are in equilibrium before the phase transition starts to take place. To fix the boundary condition for particles originating inside the bubble we assume that at $z^w \gg l_w$ there is an identical parallel wall traveling in the opposite direction. To find the abundance at ($z^w \gg l_w$, $p_z^w < 0$), we first compute the solutions along curves starting at ($z^w \ll -l_w$, $p_z^w > m_\chi^{\rm in}$) and find the abundance deep inside the bubble, at ($z^w \gg l_w$, $p_z^w > 0$). We then impose a periodic boundary condition at $z^w \gg l_w$,

$$\mathcal{A}(z^w \gg l_w, p_z^w) = \mathcal{A}(z^w \gg l_w, -p_z^w)\,. \tag{S20}$$

We neglect the effect of the wall velocity in this boundary condition, which is a small modification.